J Mater Sci: Mater Med (2010) 21:173–181
DOI 10.1007/s10856-009-3841-y

Production and characterization of HA and SiHA coatings

Qian Tang · Roger Brooks · Neil Rushton · Serena Best

Received: 12 March 2009 / Accepted: 25 July 2009 / Published online: 12 August 2009

Abstract Plasma sprayed hydroxyapatite (HA) coatings on metallic prostheses have been used clinically in dentistry and orthopedics since the mid 1980s. The coating properties are dependent on the spraying parameters. Since silicon-substituted hydroxyapatite (SiHA) has been shown to offer improved bioactivity over phase pure HA, SiHA coatings have the potential for enhanced performance in clinical application. In this study, phase pure HA and 0.8 wt% SiHA powders were synthesized with similar particle size distribution and morphology. The powders were plasma sprayed onto Ti–6Al–4V substrates at 37 kW and 40 kW plasma gun input power respectively. Four kinds of samples were prepared, HAC 37, HAC 40, SiHAC 37 and SiHAC 40. Materials characterization showed that the coatings were of relatively high phase purity. In vitro cell culture demonstrated that human osteoblast cells grew well on all samples, with the highest cell growth observed on SiHA coatings produced under the lower plasma gun input power.

1 Introduction

The number of patients requiring and receiving bone and joint replacement surgery is constantly increasing. In the United States and in Europe, more than 1 million hip and knee arthroplasties are performed each year, and this figure is continually increasing [1]. Hydroxyapatite (HA) coatings on metallic prostheses have been studied widely for major load-bearing applications due to the combination of advantages of the mechanical properties of metals and the bioactivity of HA. HA coatings can enhance bone growth across a gap of 1 mm between the bone and the implant [2], and can also limit the formation of fibrous membrane [3]. Most clinical experience shows promising results both shortly after the implantation and with continued fixation for up to 20 years [4]. Several techniques have been proposed to produce HA coatings on metallic substrates, such as sol–gel deposition [5, 6], electrophoretic deposition [7, 8] magnetron sputtering deposition [9, 10], ion-beam deposition [11, 12] and so on. Plasma spraying is currently the most widely used technique for production of commercial biomedical coatings. The properties of the coatings are dependent on very large number of spraying parameters. However, for economic and theoretical reasons, only 8–12 parameters are routinely controlled to obtain desired coating properties [13]. These parameters include plasma gun input power, composition of plasma gas, stand-off distance and the characteristics of feed materials. It is reported that silicon-substituted hydroxyapatite (SiHA) can improve the rate of bone apposition significantly compared with phase pure HA [14]. However, little research on plasma sprayed SiHA coatings has been reported.

In this study, both HA and SiHA powders were synthesized and coated on Ti–6Al–4V substrates using vacuum plasma spraying (VPS). Some physical coating properties were characterized and compared for the two compositions and an in vitro AlamarBlue test was performed. The influence of the plasma gun input power was also studied.

Q. Tang · S. Best (✉)
CCMM, Department of Materials Science and Metallurgy, University of Cambridge, Cambridge, UK
e-mail: smb51@cam.ac.uk

Q. Tang
e-mail: qt203@cam.ac.uk

R. Brooks · N. Rushton
Orthopaedic Research Unit, University of Cambridge, Box 180, Addenbrooke's Hospital, Hills Road, Cambridge CB2 2QQ, UK

2 Materials and methods

Phase pure HA was produced using a reaction between calcium hydroxide, $Ca(OH)_2$ and orthophosphoric acid, H_3PO_4, solution through a wet precipitation method [15]. SiHA was prepared using a similar method, except that tetraethyl orthosilicate (TEOS) was introduced into the H_3PO_4 solution [16]. Both HA and SiHA powders were characterized using particle size analyser, XRD, FTIR and SEM. The Si content of SiHA was measured using X-ray fluorescence (XRF).

The particle size analysis was performed using a Malvern Mastersizer 2000. Approximately 2 g HA powder was dispersed in deionised water. A Hydro 2000 MU pump was used to pump the mixture through the laser beam. The pump speed was 2000 rpm, and the ultrasonic displacement was 10 μm.

HA and SiHA powders were examined by X-ray diffraction using Philips PW 1730 diffractometer and Cu Kα radiation. The X-ray generator operated at 40 KV and a current of 40 mA. A divergence and anti-scatter slit size of 0.5° and a receiving slit of 0.2 mm were selected. Each diffraction was run from 20–40° (2θ), with a step size of 0.04 and a scan step time of 6.65 s. The peaks were identified by comparing with HA standard ICCD diffraction patterns: No. 89-4405.

FTIR was used to analyse the functional groups of the powders. The infrared spectra were recorded by a Bruker Optics Tensor 27 Fourier transform infrared spectroscopy. The absorbance of infrared waves was measured for wave numbers from 400 to 4000 cm^{-1} with the resolution of 4 cm^{-1}. OPUS software was used to collect and analyze data.

A JEOL 5800LV SEM was used to observe the microstructure of HA and SiHA powders. The electron beam was 15 KeV and all images were taken using secondary electron mode. A small amount of powder was attached onto a 12.5 mm SEM stub using double-sided conducting tape, and spread with a spatula to produce an HA layer which was uniform and thin. Since HA is not conductive, the stub was sputter coated with gold (Au) for 1 min.

Titanium alloy strips (Ti–6wt% Al–4wt% V, obtained from Allegheny Technologies Limited) were used as substrates. Plasma spraying was carried out in a Plasma Technik P1800 vacuum plasma spray unit. Four batches of samples were prepared as Table 1.

The other parameters are listed below:

Chamber Pressure: 200 mbar
Primary gas (Ar) flow rate: 50 slpm
Stand-off distance: 260 mm
Plasma gun speed: 55 mm/s

Table 1 Vacuum plasma spraying parameters

Sample	Powders used	Input power of plasma gun (kW)	Secondary gas (H_2) flow rate (slpm)
HAC 37	HA	37	4
HAC 40	HA	40	6
SiHAC 37	SiHA	37	4
SiHAC 40	SiHA	40	6

HA and SiHA coatings were examined by X-ray diffraction using the same methodology that was described for the powders. The peaks were identified by comparing with the standard ICCD diffraction patterns: HA: No. 89-4405; CaO: No. 75-0264; α-tricalcium phosphate (α-TCP): No. 86-1585; and tetracalcium phosphate (TTCP): No. 25-1137.

Coatings were detached from the substrates and ground into powder. FTIR characterization was performed with the method described previously for the powders.

The SEM samples were prepared in two ways. In both ways, the coated titanium alloy strips were cut into small pieces with a Struers Accutom-5. To analyze the morphology of the coating, the small pieces were attached to 32 mm SEM stubs using double-sided conducting tape, and then sputter coated with palladium (Pd) for 30 s. To analyze the coating/substrate interface, the cut pieces were embedded in conducting resin using quick cold mounting, and polished and etched in dilute orthophosphoric acid (about 10%) for 30 s, the stubs were sputter coated with palladium for 30 s. The JEOL 5800LV SEM was used to observe the microstructure of HA coatings. The electron beam voltage was 15 KeV and images were taken using secondary electron mode.

In vitro experiment samples were 10 mm diameter discs which were prepared according to the methods described above. Human osteoblast-like cells (HOB) isolated from trabecular bone were seeded on all samples and cultured in 1 ml McCoy's 5A medium, supplemented with 10% fetal calf serum, 1% glutamine and vitamin C (30 μg/ml) The metabolic activity of the cells was assessed by AlamarBlue assay (Serotec, Oxford, UK) at day 1, 3, 6, 9 and 12. Six replicates were used for each sample type.

3 Results and discussion

The particle size distributions of HA and SiHA powders are shown in Fig. 1 The volume weighted average particle sizes of the two kinds of powders are 75 μm and 83 μm. HA powders were similar in dimensions, but had a slightly broader distribution.

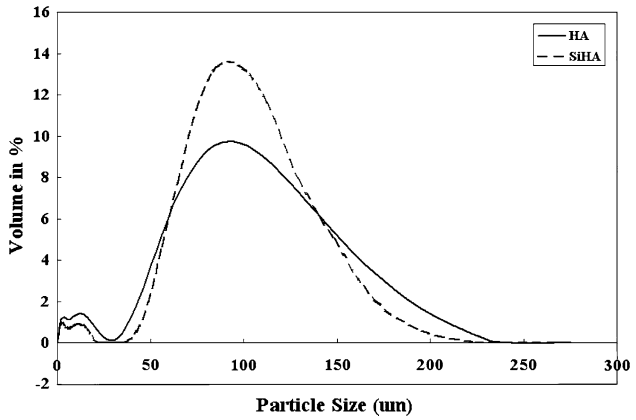

Fig. 1 Particle size distribution of HA and SiHA powders

Figure 2 illustrates the shape and size of the HA and SiHA powders. The two kinds of powders had a similar morphology. The particles were angular in shape with an average aspect ratio of about 1.5 for HA and 2.0 for SiHA.

Figures 3 and 4 show the XRD patterns of HA and SiHA powders and coatings in the range of 2θ between 20° and 40°. The purity of HA powders was high, and no peaks associated with impurities, such as TCP or CaO were evident. The XRD pattern of SiHA powders was quite similar to that of HA. The peak at 38.50° might be related to the aluminum sample holder.

According to Fig. 3, the HA coatings were nearly phase pure HA. After spraying, trace impurities appeared in the materials including α-TCP, TTCP and CaO. The plasma spray process involves two stages: (1) the change of droplet chemistry in the plasma; and (2) the formation of splats by impaction of melted particles on the substrate [17]. When hydroxyapatite particles are injected into the plasma jet, their periphery is heated to a higher temperature than the core. A chemical change occurs in the outer shell and proceeds towards the centre. At about 900°C, HA decomposes into oxyhydroxyapatite (OHA), following Eq. 1 [18].

$$Ca_{10}(PO_4)_6(OH)_2 \rightarrow Ca_{10}(PO_4)_6(OH)_{2-2x}O_xV_x + xH_2O \quad (1)$$

where V is a vacancy.

Between 1100°C and 1500°C, depending on water vapour pressure, OHA decomposes into TCP, TTCP and CaO. The reaction can be described as Eqs. 2 and 3.

$$Ca_{10}(PO_4)_6(OH)_{2-2x}O_xV_x \rightarrow 2Ca_3(PO_4)_2 + Ca_4(PO_4)_2O + (1-x)H_2O \quad (2)$$

$$Ca_4(PO_4)_2O \rightarrow Ca_3(PO_4)_2 + CaO \quad (3)$$

When the particle impacts the substrate, the TCP, TTCP and CaO phases can either react together to form HA or

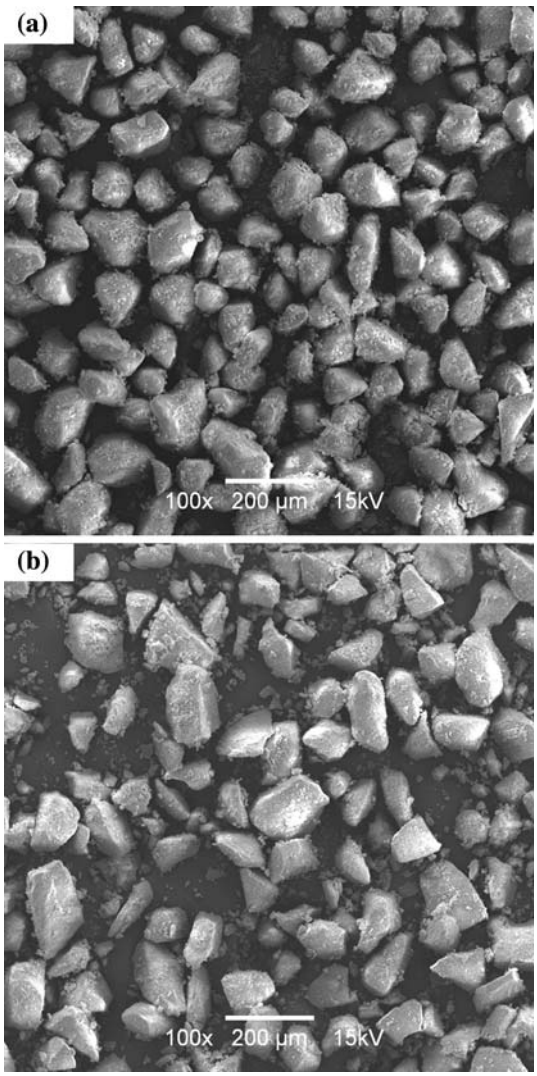

Fig. 2 Morphology of **a** HA powders and **b** SiHA powder particles

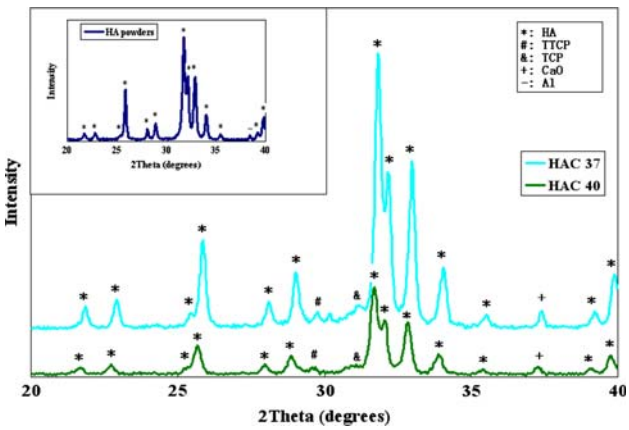

Fig. 3 XRD patterns of HA powders, HAC 37 and HAC 40

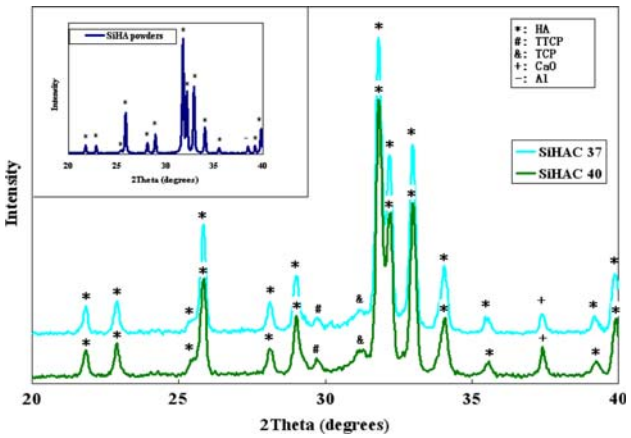

Fig. 4 XRD patterns of SiHA powders, SiHAC 37 and SiHAC 40

remain as residues. The OHA also can transform to HA by hydrolysis or remain residual. [18].

The XRD patterns of SiHA coatings were similar to the HA coatings, indicating similar reactions took place on SiHA powders during the plasma spraying processes.

The Ca, P and Si content in SiHA powders and coatings are listed in Table 2 in the form of oxides. The silicon content in the coatings was smaller than that in the powders, indicating the decomposition of SiHA during vacuum plasma spraying. Increasing the plasma gun input power, a higher percentage of SiHA decomposed, resulting in reduced silicon content.

In plasma spraying, particles within a critical size range are melted to liquid droplets. Large particles above the critical size are only partially melted [19]. These particles interact with the surrounding atmosphere and impact on the relatively cooler substrate at high velocity and form the coating. Due to the rapid cooling, the crystallization process may be limited to some extent. An amorphous phase may be formed. The crystallinity is influenced by the remaining original crystalline phase and the degree of supercooling. As the quantity of the remaining original crystalline phase increases and/or the degree of supercooling decreases, the crystallinity of the coating is increased. Higher input power is beneficial for particle melting, leading to less original crystalline phase remaining and a higher degree of supercooling. All of the coatings had high crystallinity. However, in the XRD patterns, the peaks associated with HAC 40 were lower and broader as compared with HAC 37, indicating that HA coatings produced

Table 2 The Ca, P and Si content in SiHA powders and coatings

	SiHA powders	SiHAC 37	SiHAC 40
CaO (wt%)	55.16	63.01	63.79
P_2O_5 (wt%)	40.91	35.34	34.19
SiO_2 (wt%)	1.44	0.815	0.733

at 40 kW were less crystalline than those produced at 37 kW. For commercial HA coatings, there is no agreement on the crystallinity, which can be vary from 50% to 90% (usually around 70%) [4]. According to ISO Standard 13779-2 [20, 21] ISO 13779-2 Implants for surgery—hydroxyapatite—part 2: coating of hydroxyapatite. International Organization for Standardization, 'the crystalline content of HA shall be not less than 45% and the maximum allowable level of other crystalline phases shall be 5%, with the balance being amorphous.' Therefore the phase content and the crystallinity characteristics of the plasma sprayed HA coatings produced in this study surpassed those demanded by the standard.

Fourier transform infrared spectroscopy is widely used to characterize functional groups in biomaterials. Free PO_4^{3-} ions possess tetrahedral (Td) symmetry and theoretically, they have four vibrational modes: v_1 at 938 cm^{-1} belongs to a non-degenerate P–O stretching mode, v_2 at 420 cm^{-1} belongs to a doubly degenerate bending mode, v_3 at 1017 cm^{-1} and v_4 at 567 cm^{-1} belong to triply degenerate P–O stretching and bending mode [21]. However, when PO_4^{3-} group are located in a hydroxyapatite lattice, the symmetry is lowered and the vibrational spectral patterns are altered.

Figures 5 and 6 show the FTIR spectra of HA and SiHA powders and coatings from 400 to 4000 cm^{-1}. For HA powders, v_3 band with the highest intensity is present in the region of 1016 and 1094 cm^{-1}. v_1 band is present at 961 cm^{-1}. v_4 band is split into two sharp and well defined peaks at 566 and 603 cm^{-1}. The splitting of v_4 band indicates the low site symmetry of HA molecules [22]. Compared with v_3 and v_4, v_2 band in the region of 400 and 475 cm^{-1} is relatively weak. The sharp peak at 3572 cm^{-1} can be assigned to the lattice O–H stretching vibration. The band at 633 cm^{-1} belongs to the O–H flexural mode.

Although the spectrum for SiHA powders showed all of the characteristic absorption bands for HA, the band intensity at 563 cm^{-1} and 1032 cm^{-1} corresponding to P–O decreased significantly. These changes indicated that the phosphate groups were partially replaced by silicate groups.

Hydroxyapatite contains water in both adsorbed and lattice (structural) forms. As the temperature increases, the lattice water is lost gradually. The dehydration product is oxyhydroxyapatite (OHA) below 1100°C and oxyapatite (OAP) above 1100°C. Since the crystal structures of OHA and OAP are quite similar to that of HA, the dehydration can not be detected with XRD. Therefore, FTIR spectroscopy is used. The significant decrease of 3572 cm^{-1} peak can be explained by the dehydration. The peak in HAC 40 was slightly lower than those in HAC 37, indicating a more intense dehydration.

Comparing to HA powders, the peaks corresponding to P–O in HA coatings were lower and broadened. The peaks

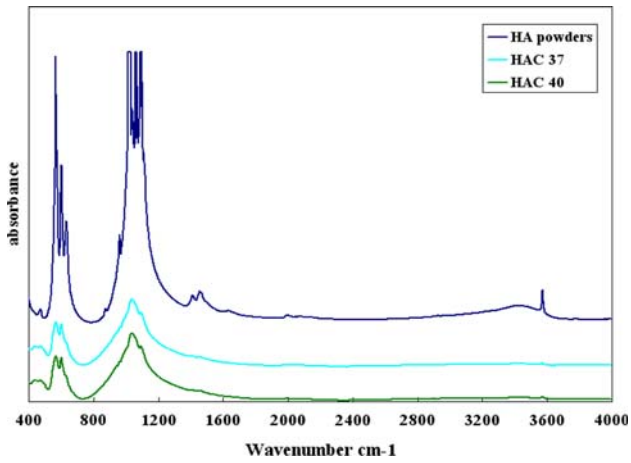

Fig. 5 FTIR spectra of HA powders, HAC 37 and HAC 40

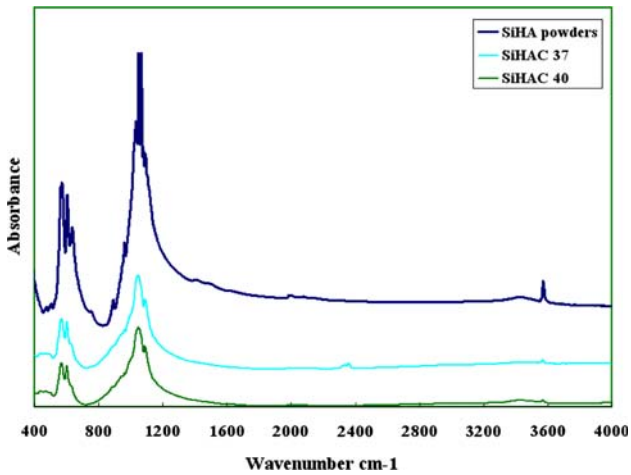

Fig. 6 FTIR spectra of SiHA powders SiHAC 37 and SiHAC 40

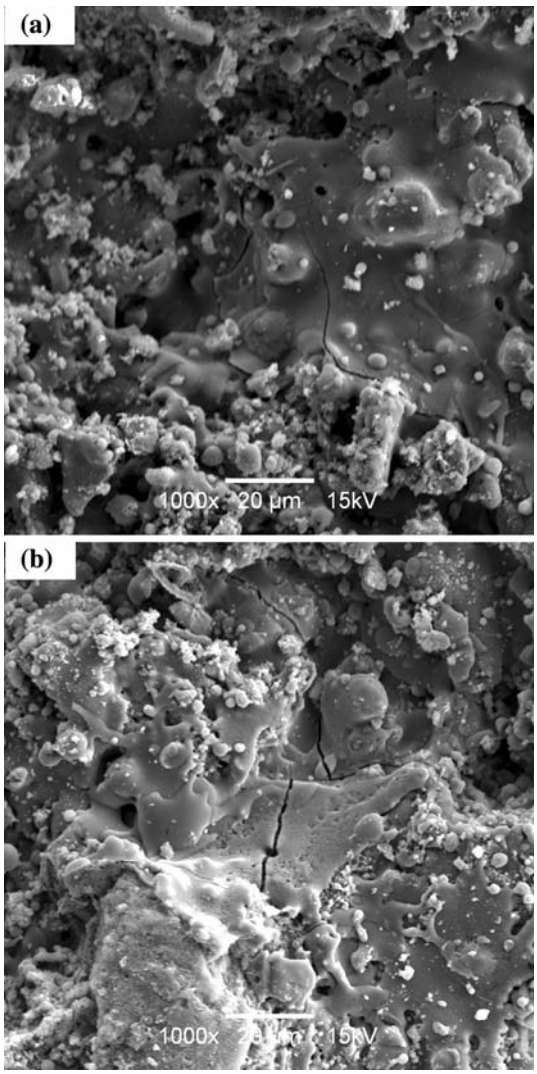

Fig. 7 Morphology of **a** HAC 37 and **b** HAC 40

at around 961 cm^{-1} and 1093 cm^{-1} significantly decreased. This might be attributed to the presence of the amorphous HA phases. The FTIR spectra of SiHAC 37 and SiHAC 40 have a similar change trend to HAC 37 and HAC 40. This confirmed the dehydration of SiHA powders and the formation of amorphous phase during vacuum plasma spray.

The surface morphology of HA and SiHA coatings can be obtained by SEM, which are shown in Figs. 7 and 8. Both HA and SiHA coatings formed by the superposition of the molten particles (flat splats) displayed a rough, irregular and inhomogeneous morphology. On the flattened splats, there were some small particles. This may be due to the fine particles in the starting powders, which were melted into small liquid droplets and deposited on large splats.

Before plasma spraying, the substrate was grit blasted with alumina in order to provide mechanical anchorage points for the deposited layer. This substrate preparation may contribute to the inhomogeneity of the coating [23]. Cracks were present along the coating surface, which might be caused by the shrinkage of the splats during cooling and subsequent differential thermal contraction between the substrate and coating. The width of the cracks was usually less than 1 µm. At high magnification, the cracks spread either across or along the splats.

Figures 7 and 8 showed that particles sprayed at 40 kW melted more completely. A higher number of flattened splats were observed in HAC 40 and SiHAC 40 than for HAC 37 and SiHAC 37. Higher plasma gun input power resulted in higher heat content of the plasma and provided more ability to melt the particles. Under the same plasma spray conditions, HA powders melted more completely. This may be due to subtle differences in the particle size distribution for the HA powders as compared with the

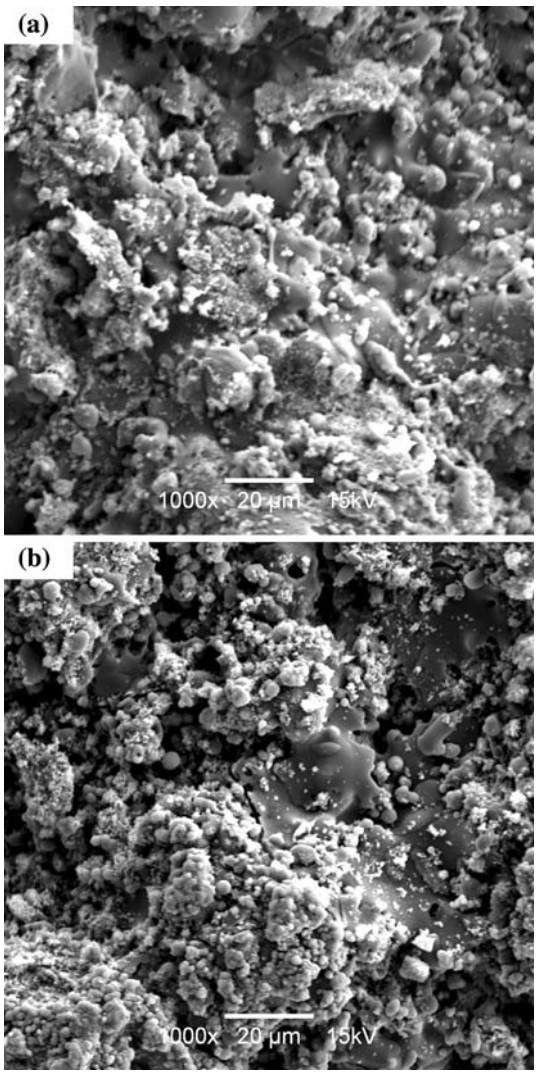

Fig. 8 Morphology of **a** SiHAC 37 and **b** SiHAC 40

SiHA powders, since small powders particles are more prone to melting. However, it may also be as a result of silicate groups in the SiHA crystal lattice which increased the melting temperature of the material. Patel et al. [14] found that the sintering temperature required for SiHA is higher than for pure HA [24].

The cross sections of the HA and SiHA coatings are shown in Figs.9 and 10. The thickness of the coatings was approximately 100 µm. For all coatings, no obvious cracks appeared at the coating/substrate interface. The cross sectional SEM images confirmed that power sprayed at higher plasma gun input power underwent a higher degree of melting and the SiHA powders did not melt to the same degree as HA powders under equivalent VPS conditions.

The metabolic activity of HOBs on all samples is shown in Fig. 11. HOBs appeared to grow very well on HAC 37 and SiHAC 37, since the metabolic activity increased with culturing time. Cell responses were also compared between different samples at each time point. Comparing HAC 37 and HAC 40, or SiHAC 37 and SiHAC 40, cells grew better on coatings produced at 40 kW from day 1–3, but the differences were not sufficient to be considered significant. From day 6, the HOB cells showed higher metabolic activity on coatings produced at 37 kW, and a significant difference was observed at days 9 and 12. Considering the whole culturing period, HA and SiHA coatings produced at 37 kW were more supportive to HOB cell growth than those produced at 40 kW.

The bioactivity of HA is proposed to follow a dissolution–precipitation mechanism. After implantation, HA dissolves, leading to the increase of the concentration of calcium and phosphate ions in the spaces between bone and the implant [25], and then a new apatite-like phase is developed into this space, which incorporates the implant

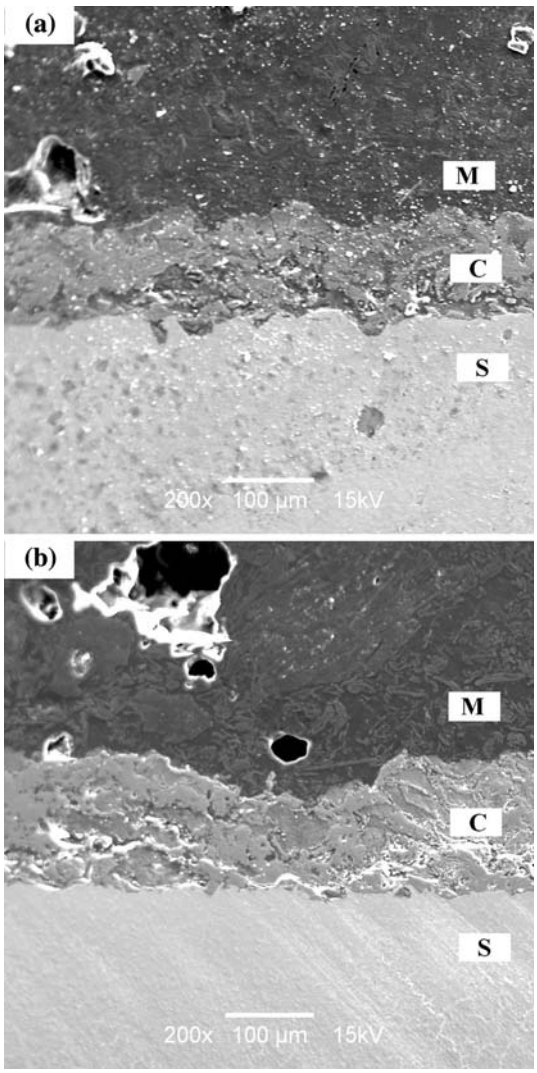

Fig. 9 Cross section of **a** HAC 37 and **b** HAC 40. M: mounting resin, C: coating, S: Substrate

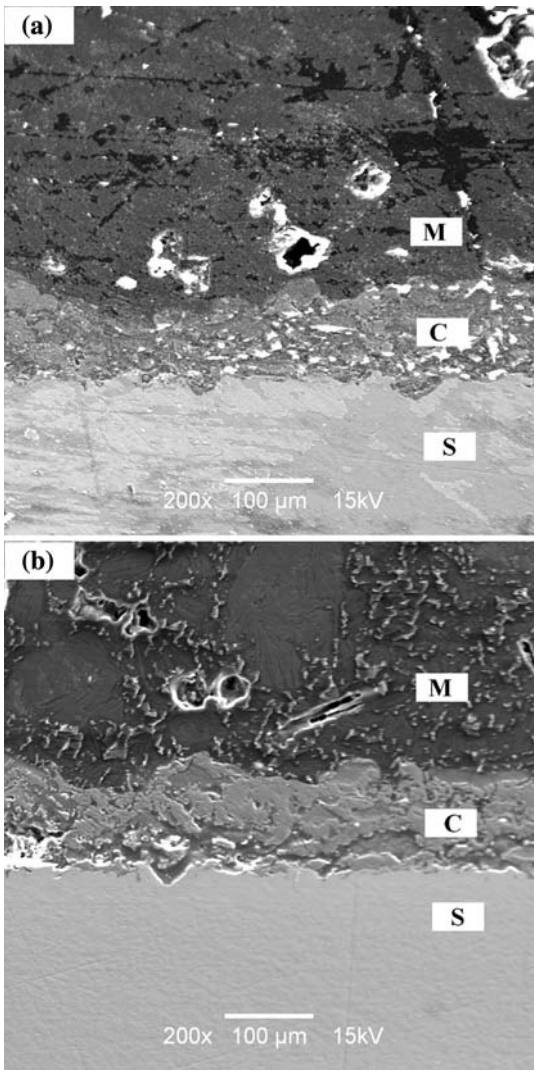

Fig. 10 Cross section of **a** SiHAC 37 and **b** SiHAC 40. M: mounting resin, C: coating, S: Substrate

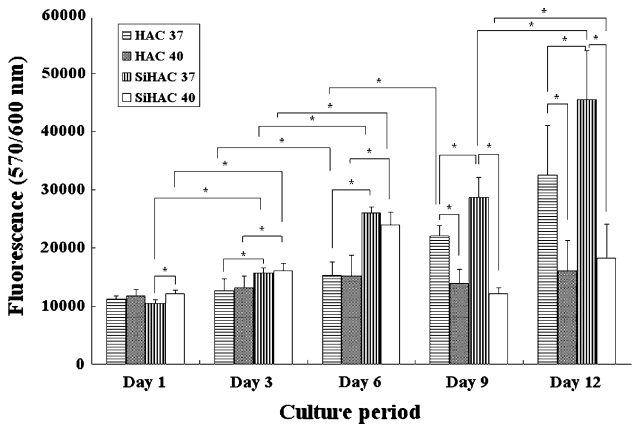

Fig. 11 Metabolic activity of HOBs on all samples surfaces versus culturing time * $P < 0.05$

and the existing bone [26]. The rate of new apatite layer formation can be considered as a criterion for bioactivity measurement. As described above, plasma sprayed HA and SiHA coatings contained a small amount of amorphous phase, impurities, such as CaO, TCP, TTCP. All of these components are substantially more soluble than the crystalline HA and SiHA. In the beginning, HOBs showed a better attachment and growth on HAC 40 and SiHAC 40, which were more soluble due to the impurities compared with HAC 37 and SiHAC 37 respectively. However, this did not result in a higher metabolic activity in the following few days. The finding may be due to the fact that HAC 40 and SiHAC 40 dissolved too rapidly to support cell growth. It was also assumed that an alkaline pH of the culture medium, caused by dissolution of the soluble impurities, might have a cytotoxic effect inhibiting the proliferation of attached cells [27]. An alkaline pH may also lead to a cytotoxic effect inhibiting DNA and protein synthesis in tissue culture. While the mineralization will be increased by elevated amounts of soluble components derived from the coatings, the side-effect of consequent pH change at the interface on the cell growth should also be of concern [27]. Further studies are required on the relationship between pH change and cell growth to optimize the surface crystallinity for both cell growth and mineralization at the bone/coating interfaces.

The improvement of bioactivity of SiHA compared with HA can be explained by combining the following factors. The incorporation of silicate groups into the HA lattice leads to a tetrahedral distortion. The incorporation of silicate ions creates some hydroxyl site vacancies, which decreases the apatite structure stability and in turn increase the reactivity. Porter et al. used HR-TEM to characterize the defects, e.g. dislocations, grain boundaries and triple junctions in HA and SiHA. More triple junctions and subgrain boundaries were found in SiHA than HA [28]. It was reported dissolution initiated from and was particularly prevalent at grain boundaries and triple junctions in vivo [29]. Therefore, the increase in number of defects may be the mechanism by which the incorporation of silicate ions increases the solubility of HA and subsequently improves the bioactivity. Since the bioactivity process is a surface process between the material and the living tissue, the chemical changes of the surfaces caused by the introduction of silicate ions may influence the bioactivity. It is believed that the substitution of SiO_4^{4-} for PO_4^{3-} creates a more electronegative surface, which facilitates HA dissolution. [30] Gibson et al. seeded human osteosarcoma (HOS) cells on HA and SiHA samples. The in vitro test showed that the metabolic activity of HOS cells on SiHA was higher than for HA at all time points. [31] In this study, considering HA and SiHA coatings produced under the same VPS conditions, there was enhanced cell growth on

the SiHA coatings and thus the results appear to confirm that silicon stimulates cell growth.

4 Conclusions

Hydroxyapatite and silicon substituted hydroxyapatite were synthesized in the laboratory and the resulting powders were vacuum plasma sprayed onto Ti–6Al–4V substrates. The powders and coatings were characterized with XRD, FTIR and SEM. An AlamarBlue assay was used to test the HOB cells metabolic activity. The conclusions have been drawn as follows:

- Phase pure HA and SiHA powders were produced in-house with similar particle size morphology.
- HA and SiHA coatings were produced successfully in terms of composition, crystallinity, microstructure and coating/substrate bonding.
- The coatings exhibited similar levels of phase purity.
- Increasing plasma gun input power led to better melting of the powders, but dehydroxylation and silicon loss was increased.
- Under the same conditions, SiHA powders were not melted as completely as HA powders.
- SiHAC 37 exhibited the highest cell growth support among all samples throughout the culturing period.

Acknowledgements The authors acknowledge Mr. Kevin Roberts for his kind assistance with sample preparation (carrying on plasma spray), and Prof. Bill Clyne for his suggestions and the use of facilities. The British Government for ORS funding, and Cambridge Overseas Trust and Trinity College for funding for Qian Tang Dr. Roger Brooks acknowledges funding from the National Institute for Health Research.

References

1. Heimann RB. Thermal spraying of biomaterials. Surf Coat Technol. 2006;201:2012–9.
2. Soballe K, Hansen ES, Rasmussen HB, Hjortdal VE, Juhl GI, Pedersen CM, et al. Gap healing enhanced by hydroxyapatite coating in dogs. Clin Orthop. 1991;272:300–7.
3. Soballe K, Hansen ES, Rasmussen HB, Bunger C. Hydroxyapatite coating converts fibrous tissue to bone around loaded implants. J Bone Joint Surg. 1993;75B:270–8.
4. Sun L, Berndt CC, Gross KA, Kucuk A. Materials fundamentals and clinical performance of plasma-sprayed hydroxyapatite coatings: a review. J Biomed Mater Res Appl Biomater. 2001;58:570–92.
5. Gross KA, Chai CS, Kannangar GS, Nissan BB. Thin hydroxyapatite coatings via sol-gel synthesis. J Mater Sci: Mater Med. 1998;9:839–43.
6. Chai CS, Gross KA, Nissan BB. Critical aging of hydroxyapatite sol-gel solutions. Biomaterials. 1998;19:2291–6.
7. Ducheyne P, Raemonck WV, Heughebaert JC, Heughbaert M. Structural analysis of hydroxyapatite coatings on titanium. Biomaterials. 1986;7:97–103.
8. Zhitomirsky I, Gal-Or L. Electrophoretic deposition of hydroxyapatite. J Mater Sci: Mater Med. 1997;8:213–9.
9. De Groot L, Wolke JGC, Jansen JA. Calcium phosphate coatings for medical implants. Proc Inst Mech Eng H J Eng Med. 1998;212:137–47.
10. Nieh TG, Jankowski AF, Koike J. Processing and characterization of hydroxyapatite coatings on titanium produced by magnetron sputtering. J Mater Res. 2001;16:3238–45.
11. Wang C, Chen Z, Guan L, Liu Z, Wang P, Zhang S, et al. Structural characterization of ion beam sputtering deposited calcium phosphate coatings. Surf Coat Technol. 2000;130:39–45.
12. Ong JL, Lucas LC. Post-deposition heat treatment for ion beam sputter deposited calcium phosphate coatings. Biomaterials. 1994;15:337–41.
13. Heimann RB. Plasma-spray coatings: principles and applications. New York: Weinheim and VCH; 1996.
14. Patel N, Brooks RA, Clarke MT, Lee PM, Rushton N, Gibson IR, et al. In vivo assessment of hydroxyapatite and silicate-substituted hydroxyapatite granules using an ovine defect model. J Mater Sci: Mater Med. 2005;6:429–40.
15. Osaka A, Miura Y, Takeuchi K, Asada M, Takahashi K. Calcium apatite prepared from calcium hydroxide and orthophosphoric acid. J Mater Sci: Mater Med. 1991;2:51–5.
16. Gibson IR, Best SM, Bonfield W. Chemical characterization of silicon-substituted hydroxyapatite. J Biomed Mater Res. 1999;44:422–8.
17. Gross KA, Berndt CC, Stephens P, Dinnebier R. Oxyapatite in hydroxyapatite coatings. J Mater Sci. 1998;33:3985–91.
18. Carayon MT, Lacout JL. Study of the Ca/P atomic ratio of the amorphous phase in plasma-sprayed hydroxyapatite coatings. J Sol Stat Chem. 2003;172:339–50.
19. Cheang P, Khor KA. Addressing processing problems associated with plasma spraying of hydroxyapatite coatings. Biomaterials. 1996;17:537–44.
20. Lima RS, Khor KA, Li H, Cheang P, Marple BR. HVOF spraying of nanostructure hydroxyapatite for biomedical applications. Mater Sci Eng A. 2005;396:181–7.
21. Park E, Condrate RA, Lee SD. Infrared special investigation of plasma spray coated hydroxyapatite. Mater Lett. 1998;36:38–43.
22. Rehman I, Bonfield W. Characterization of hydroxyapatite and carbonated apatite by photo acoustic FTIR spectroscopy. J Mater Sci: Mater Med. 1997;8:1–4.
23. Garcia-Sanz FJ, Mayor MB, Arias JL, Pou J, Leon B, Perez-Amo M. Hydroxyapatite coatings: a comparative study between plasma-sprayed and pulsed laser deposition techniques. J Mater Sci: Mater Med. 1997;8:861–5.
24. Patel N, Follon EL, Gibson IR, Best SM, Bonfield W. Comparison of sintering and mechanical properties of hydroxyapatite and silicon-substituted hydroxyapatite. Key Eng Mater. 2003;240–242:919–22.
25. Weng J, Liu Q, Wolke JGC, Zhang X, De Groot K. Formation and characteristics of apatite layer on plasma-sprayed hydroxyapatite coatings in simulated body fluid. Biomaterials. 1995;18:1027–35.
26. Porter AE, Botelho CM, Lopes MA, Santos JD, Best SM, Bonfield W. Ultrastructural comparison of dissolution and apatite precipitation on hydroxyapatite and silicon-substituted hydroxyapatite in vitro and in vivo. J Biomed Mater Res. 2004;69A:670–9.
27. Chou L, Marek B, Wagner WR. Effects of hydroxyapatite coating crystallinity on biosolubility, cell attachment efficiency and proliferation in vitro. Biomaterials. 1999;20:977–85.

28. Porter AE, Best SM, Bonfield W. Ultrastructural comparison of hydroxyapatite and silicon-substituted hydroxyapatite for biomedical applications. J Biomed Mater Res. 2004;68A:133–41.
29. Porter AE, Patel N, Skepper JN, Best SM, Bonfield W. Comparison of in vivo dissolution process in hydroxyapatite and silicon-substituted hydroxyapatite bioceramics. Biomaterials. 2003;24:4609–20.
30. Vallet-Regi M, Daniel A. Silicon substituted hydroxyapatites. A method to upgrade calcium phosphate based implants. J Mater Chem. 2005;15:1509–16.
31. Gibson IR, Huang J, Best SM, Bonfield W. Enhanced in vitro cell activity and surface apatite layer formation on novel silicon-substituted hydroxyapatites. Bioceramics. 1999;12:191–4.